A Particle X-ray Temporal Diagnostic (PXTD) for studies of kinetic, multi-ion effects and ion-electron equilibration rates in Inertial Confinement Fusion plasmas at OMEGA[a)]

H. Sio,[1,b)] J.A. Frenje,[1] J. Katz[2], C. Stoeckl[2], D. Weiner[2], M. Bedzyk, V. Glebov[2], C. Sorce[2], M. Gatu Johnson[1], H. G. Rinderknecht[4], A. B. Zylstra[3], T. C. Sangster[2], S. P. Regan[2], T. Kwan[3], A. Le[3], A. N. Simakov[3], W. T. Taitano[3], L. Chacòn[3], B. Keenan[3], R. Shah[3], G. Sutcliffe[1], and R.D. Petrasso[1]

[1]*Plasma Science and Fusion Center, Massachusetts Institute of Technology, Cambridge, MA, 02139, USA*
[2]*Laboratory for Laser Energetics, University of Rochester, Rochester, NY, 14623, USA*
[3]*Los Alamos National Laboratory, Los Alamos, NM, 87545, USA*
[4]*Lawrence Livermore National Laboratory, Livermore, CA 94550, USA*

(Presented XXXXX; received XXXXX; accepted XXXXX; published online XXXXX)

A Particle X-ray Temporal Diagnostic (PXTD) has been implemented on OMEGA for simultaneous time-resolved measurements of several nuclear products as well as the x-ray continuum produced in High Energy Density Plasmas (HEDP) and Inertial Confinement Fusion (ICF) implosions. The PXTD removes systematic timing uncertainties typically introduced by using multiple instruments, and it has been used to measure DD, DT, D^3He, and T^3He reaction histories and the emission history of the x-ray core continuum with relative timing uncertainties within ± 10-20 ps. This enables, for the first time, accurate and simultaneous measurements of the x-ray emission histories, nuclear reaction histories, their time differences, and measurements of $T_i(t)$ and $T_e(t)$ from which an assessment of multiple-ion-fluid effects, kinetic effects during the shock-burn phase, and ion-electron equilibration rates can be made.

I. INTRODUCTION

In an Inertial Confinement Fusion (ICF) implosion, shocks propagate through the low-density fuel and set up the initial conditions for deceleration and hot-spot formation. During the shock propagation phase of the implosion, the ion-ion mean-free-path in the fuel is on the order of the implosion radius due to high temperature and low density, which makes the plasma highly kinetic. At the same time, radiation-hydrodynamic codes incorrectly treat multiple ion species as a single average-mass, average-charge ion species. Because of these not-modeled but important physics, the hydrodynamic treatment is not sufficient to capture the relevant implosion physics during the shock phase.

Recent experimental studies also indicate that kinetic and multi-ion-fluids effects have measurable impacts on the implosion performance, especially during the shock phase in an ICF implosion. Observations in these experiments include: yield degradation as the implosion becomes more kinetic[1], thermal decoupling between ion species[2], anomalous yield scaling for different plasma mixture[3,4], ion diffusion[5], and fuel stratification[6]. One common theme in these studies is that they are based on time-integrated nuclear observables such as yields and burn-averaged ion-temperatures. A natural extension of these studies is therefore to conduct precision measurements of multiple nuclear burn histories. The role of kinetic and multi-ion-fluid effects in ICF plasmas can be studied in a time-resolved sense using relative timing of peak burn, burn duration, and evolution of the yield ratio between different nuclear reactions. As multi-ion-fluid and/or kinetic-ion simulations (such as LSP[17]) are becoming increasingly sophisticated, quantitative comparisons with experimentally measured nuclear reaction histories will also be made in the near future.

This work describes the development and implementation of the Particle X-ray Temporal Diagnostic (PXTD) on OMEGA[7] for time-resolved high-precision measurements of multiple nuclear-reaction yields. The same configuration can also be used to simultaneously measure multiple x-ray emission histories to probe the x-ray core continuum. This diagnostic is an extension of the Particle Temporal Diagnostic (PTD)[8]. Using the PXTD for these measurements enables excellent relative timing precision between the measured nuclear and x-ray emission histories (± 10-20 ps) by eliminating jitters and cross-timing issues, normally seen between different diagnostics. This enables accurate and simultaneous measurement of the peak x-ray emission time and peak nuclear production time (x-ray and nuclear bang-time, respectively), their time differences, and measurements of $T_i(t)$ and $T_e(t)$ from which an assessment of multiple-ion-fluid effects, kinetic effects during the shock-burn phase, and ion-electron equilibration rates can be made.

The structure of this paper is as follows. Section II describes the PXTD design and performance. Section III discusses the different measurements of the nuclear-reaction and x-ray-emission histories. Section IV elaborates on the different analysis methods and measurement uncertainties on the determined nuclear and x-ray signatures. Section V discusses a

a) Invited paper published as part of the Proceedings of the 21st Topical Conference on High-Temperature Plasma Diagnostics (HTPD 2016) in Madison, Wisconsin, USA.
b) Author to whom correspondence should be addressed: hsio@mit.edu

new PXTD design to further reduce measurement uncertainties by positioning the detector closer to the implosion. Section VI concludes and discusses the path forward.

II. PXTD DESIGN AND PERFORMANCE

The Neutron Temporal Diagnostic (NTD)[9] on the NOVA[10] was the first nuclear emission history diagnostic implemented on a laser facility. This was followed by the OMEGA NTD, and the Ten-Inch-Manipulator-based cryoNTD[11]. Modification to the nosecone and filtering of the cryoNTD led to the Particle Temporal Diagnostic (PTD)[8], which was designed to measure either the D^3He-p or the DD-n burn history. These systems are all based on a fast organic scintillator coupled to an optical streak camera. The scintillator used is either a EJ-232 or a BC-422 with a fast rise time (< 20 ps) and long decay time (~ 1.4 ns). As the scintillator rise time is fast and the decay time is slow, the information of the emission history is encoded in the leading edge of the streaked image.

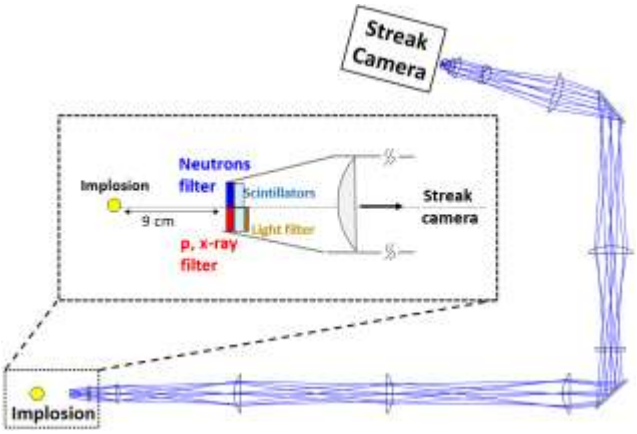

Figure 1: Schematic of the PXTD design on OMEGA, which uses a 3.5-m optical relay to transport light from the scintillators positioned at 9 cm from the implosion to an optical streak camera outside the target chamber. The front end close to the implosion is visually expanded for clarity. Either a 2-channel or 3-channel scintillator setup is used in the nosecone. The 2-channel setup shown here houses two pieces of optically isolated scintillator, with filtering in front to measure neutrons, and proton/x-ray respectively. A light attenuation filter is placed behind one of the scintillators to equalize the signals from the two channels.

The PXTD is an extension of the PTD in terms of capability. PXTD shares the same optical relay and streak camera as the PTD, and use more complex filtering and scintillator setup in the nosecone to record multiple nuclear-reaction and x-ray emission signals simultaneously. The scintillator is positioned 9 cm away from the implosion and is sensitive to charged particles, neutrons, and x-rays. The light from the scintillator is collected by a f/2 lens, transported through a 3.5-m optical-relay system, and de-magnified 3:1 onto the input plane of a fast (<15 ps) optical streak camera positioned outside the target chamber (Figure 1). The OMEGA fiducial system is used to generate a series of eight light pulses spaced 548 ps apart, which is delivered via an optical fiber and imaged onto the streak camera for an absolute timing reference. The fiducial pulses are used for absolute timing of the reaction histories, and also used to correct for sweep-speed nonlinearity in the streak camera (see Figure 3).

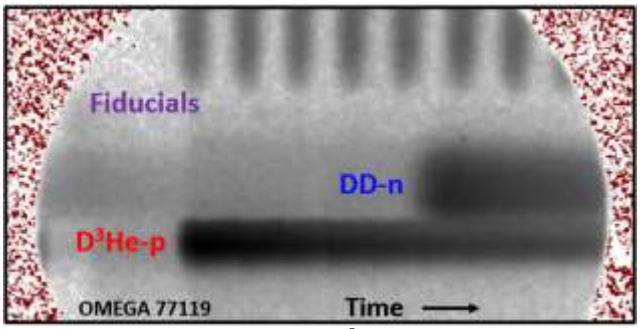

Figure 3: PXTD streak image from a D^3He-gas-filled implosion (OMEGA 77119). The streak signal is produced by the 14.7-MeV D^3He-p and 2.45-MeV DD-n from the implosion. The OMEGA fiducials, spaced 548 ps apart, appear at the top of the streak image and are used for absolute timing relative to the laser pulse.

For simultaneous measurements of the nuclear-reaction and x-ray emission histories, the PXTD front end either consists of two or three separate scintillators, each with its own filtering on the front (implosion-facing) side, and its own light attenuation filter on the back (camera-facing) side. To prevent signal overlap between the different channels, each scintillator is spatially separated by 5 mm. The different scintillator setups and examples of corresponding PXTD data are shown in Figure 2. As each channel's light level can be adjusted individually by using a different amount of Kapton light attenuation filters, two nuclear signals (D^3He-p and DD-n) with order-of-magnitude difference in signal strength can be recorded simultaneously with one streak camera (Fig. 2, top row). Similarly, several x-ray emission histories (energies above 6 keV, 12 keV, and 20 keV) can be measured simultaneously on different channels (Fig. 2, bottom row).

The main challenge when simultaneously measuring

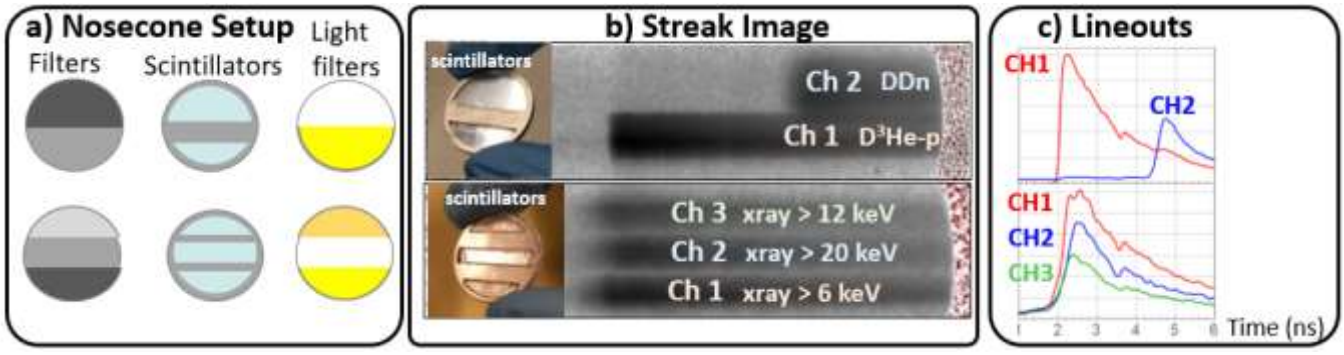

Figure 2: (a) PXTD scintillator(s), x-ray filter and light attenuation filter configurations for the different measurements. (b) Measured D^3He-p and DD-n streaks simultaneously using two channels (top row), and three measured x-ray streaks at different energy bands using three channels (bottom row). As indicated by (a), each streak channel has its own filtering in front of, and light attenuation filter behind, the scintillator to equalize the signal relative to the other channels. (c) Projected nuclear-reaction and x-ray lineouts. The filtering for the multiple nuclear reactions (top row) and x-ray emission (bottom row) cases will be discussed in details in Sec. 3a and Sec 3b, respectively.

multiple nuclear and x-ray emission histories is to keep all signals within the dynamic range of the streak camera. The reason for this is that 14.7-MeV D^3He-p produces ~600x more scintillator photons than 2.45-MeV DD-n, and ~200x more scintillator photons than 14.1-MeV DT-n. This difference is due to the fact that every proton deposits energy in the scintillator, whereas only a small fraction of neutrons interacts and deposits energy in the scintillator. For a robust simultaneous measurement of nuclear and x-ray emission histories, all signals of interest must be within a factor of five of each other, which is accomplished by adjusting each channel's optical filtering. The same design concern applies to x-ray emission histories where the Bremsstrahlung continuum signal above different cutoff energies (for instance above 6 keV, 12 keV and 20 keV) can vary up to three orders of magnitude.

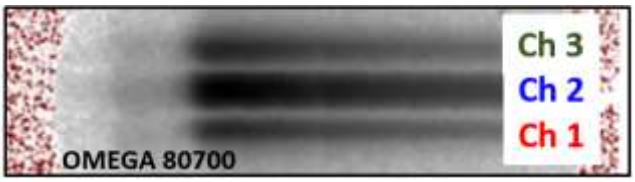

Figure 4: PXTD x-ray flat-field streak image for OMEGA shot 80700. In this experiment, all three channels use the same x-ray and light attenuation filter. Vignetting of the optical system and differences in scintillator thickness contributed approximately equally to the spatial difference in the light distribution across the different channels (along the direction perpendicular to the streak).

The motivation to measure the different x-ray emission histories is to probe the time-resolved core x-ray continuum. To accomplish this, it is critical to understand the relative efficiency of each channel. In particular, how the vignetting of the optical system causes differences in the light levels at the periphery and center of the streak signal must be understood. Nuclear reaction history measurements are insensitive to this issue as an absolute calibration of the different PXTD signals are available from other nuclear diagnostics measurements. However, understanding the relative light collection efficiency for each streak channel is especially important for measurements of x-ray emission histories as the signal ratio between the different channels is used to determine the slope of the Bremsstrahlung continuum. To address this issue, a flat-field shot is used to determine the spatial distribution of light along the axis perpendicular to the timing axis. An example of a flat-field measurement is shown Figure 4. In this measurement, the PXTD was fielded with all three channels using the same x-ray and light filters. Channel 2, which is the center channel and has a 2-mm-thick scintillator, has a relative efficiency of 1.00. Channel 1 and channel 3, on either side, have a 1-mm-thick scintillator and a relative efficiency of 0.27 and 0.30, respectively. Scintillator thickness differences reduce light collection for channel 1 and channel 3 by ~ 50%, relative to channel 2. The vignetting effect reduces light collection for channel 1 and channel 3 by ~ 40% relative to channel 2.

Additionally, the scintillator sensitivity to x-rays with different energies and the x-ray transmission through different filters must be determined to infer the slope of the Bremsstrahlung continuum of the emitted x-rays. This is done by, first, calculating the x-ray interaction probability in the scintillator using Compton scattering and photo-absorption cross sections [NIST] for polyvinyltoulene, the base polymer for the scintillator. Second, the amount of deposited energy and light generated by Compton-scattered and photo-absorption electrons are determined. Figure 5 shows an example with an x-ray source spectrum from a T_e = 3 keV plasma and the PXTD response to this source spectrum, taking into account x-ray filter transmission, energy deposition in the scintillator, and light collection efficiency of the optics (e.g. effect of vignetting). The integral of each absorption curve gives the expected relative signal level for each channel.

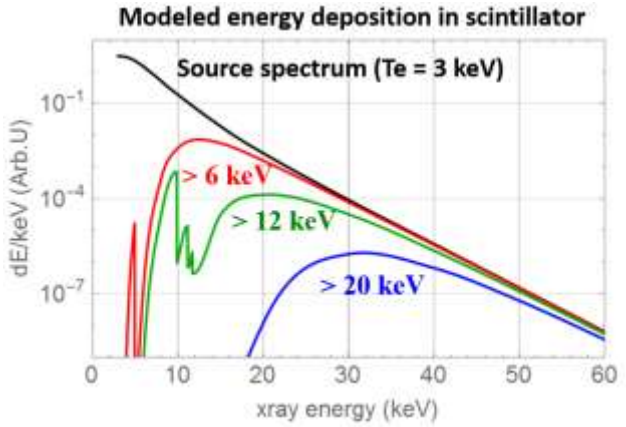

Figure 5: PXTD response to x-rays from a T_e = 3 keV plasma. Ch1 is filtered with 181-μm Al + 102-μm Ti. Ch2 is filtered with 181-μm Al + 635-μm Stainless Steel. Ch3 is filtered with 181-μm Al + 41-μm Ta. This calculation takes into account x-ray filter transmission, energy deposition in the scintillators, and light collection efficiency of the optics (e.g. effect of vignetting).

III. TIME_RESOLVED MEASUREMENTS OF THE NUCLEAR-REACTION AND X-RAY EMISSION HISTORIES

A. NUCLEAR-REACTION HISTORIES

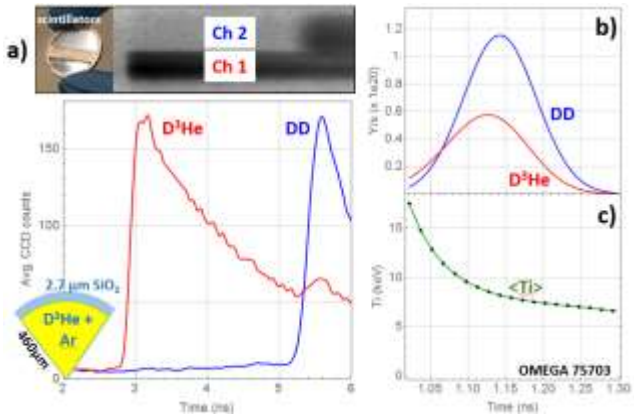

Figure 6: Simultaneous PXTD measurements of the 14.7-MeV D^3He-p and the 2.45-MeV DD-n burn histories from a thin-glass, D^3He-gas-fill implosion on OMEGA shot 75703. a) The streak image illustrates the streak of the DD-n signal (top part of image) and the D^3He-p signal (bottom-part of image). The bottom part of (a) illustrates the 14.7-MeV D^3He-p and 2.45-MeV DD-n streak lineouts (the streak image projected onto the time axis). At 9 cm away from the implosion, the D^3He-p arrives about 2.5 ns before the DD-n. b) D^3He-p and DD-n burn histories determined from the data in (a) using a forward-fitting method which includes a model of the PXTD response. (c) Time-resolved ion temperature $T_i(t)$ inferred from the ratio of the DD and D^3He nuclear reaction rates shown in (b). See text for more details.

Several nuclear reaction histories can be measured simultaneously with the PXTD by using different filtering in front of each scintillator and appropriate light filters behind each scintillator. As a typical example, Figure 6a illustrates simultaneous PXTD measurements of the 14.7-MeV D^3He-p and

the 2.45-MeV DD-n emission histories. The image in Figure 6a illustrates the streaked signal of the DD-n (top) and the D^3He-p signal (bottom). The filter used in front of the scintillator for the proton channel (Ch1) was 200-μm Ta + 100-μm Al. This channel is sensitive to both D^3He-p and DD-n, but because the scintillator is ~ 500x more sensitive to D^3He-p than to DD-n, the streak is dominated by D^3He-p signal. In the neutron channel (Ch2), a filtering of 700-μm Ta + 100-μm Al was used, which ranges out the protons and thus only sensitive to DD-n. To reduce the light of the D^3He-p and DD-n to a similar level at the streak camera, the proton channel has an 8-μm Kapton filter behind the scintillator, which attenuates the scintillator light output from the proton channel by ~ 400x.

Figure 6b shows the DD- and D^3He-reaction histories determined from the lineouts shown in (a) using a forward-fitting method which includes a model of the PXTD response. These histories have a relative timing uncertainty within ± 20 ps, which is far more accurate than can be achieved with two diagnostics because it is insensitive to diagnostic jitter and not reliant on cross-timing and timing shots. The forward-fitting method and the resulting uncertainties are discussed in Sec IV. As the DD and D^3He reactivities have different temperature sensitivities , a spatially-averaged, time-resolved ion temperature $T_i(t)$ can be inferred from the data (Figure 6c).

B. X-RAY EMISSION HISTORY

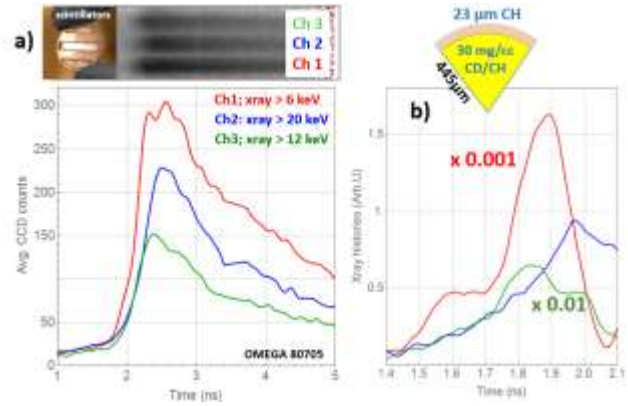

Figure 7: Simultaneous PXTD measurements of emission histories of x-rays with energies above 6 keV, 12 keV, and 20 keV from a thick-CH implosion on OMEGA. a) The top image illustrates the streak of the three x-ray signals, while the bottom plot illustrates the x-ray lineouts (the streak image projected onto the time axis). b) Deconvolved x-ray emission histories determined from the lineouts shown in (a). These emission histories were determined by considering and correcting for the PXTD response, light filter transmission, and channel efficiency. The filtering for these three channels are described in Figure 5. In b), channel 1 (red) and channel 3 (green) are scaled by 0.001, and 0.01, respectively, to display all three signals on the same scale.

Using x-ray filters with different cutoff energies, three different x-ray emission histories are measured simultaneously, with appropriate light attenuating filters behind the scintillator to bring signal levels to within the dynamic range of the streak camera. An example of x-ray emission data is shown in Figure 7a. From the x-ray lineouts shown in Figure 7a, the x-ray emission histories are determined using a deconvolution analysis technique. Removing the detector response using a deconvolution method to recover the x-ray emission histories is the preferred analysis approach because x-ray signals do not need to be corrected for Doppler-broadening, and because they may not have a well-defined shape that can be described by simple source functions. In the analysis, the data is corrected for light filter attenuation and channel light collection efficiency (Figure 7b). From the x-ray emission histories, an x-ray bang-time and burnwidth at different x-ray energies can be determined. The similar magnitudes of the three streak lineouts in Figure 7a demonstrates the application of light filter to equalize the signal magnitudes that spans three order of magnitude across the three channels.

To infer time-resolved, spatially-averaged $T_e(t)$, the slope of the time-resolved x-ray spectrum is used. At each time step, a model exponential spectrum is adjusted until a good fit to the observed signals the three channels is found. For thin-glass shock-driven implosions typically used for studies of kinetic and multi-ion-fluid effects in ICF plasmas, opacities are insignificant and can be neglected because the shell is almost entirely ablated away before nuclear production period. For the thick-CH implosion shown in Figure 7, opacity is expected to be significant, especially for the lower energy x-ray bands.

C. SIMULTANEOUS MEASUREMENTS OF NUCLEAR-REACTION AND X-RAY EMISSION HISTORIES

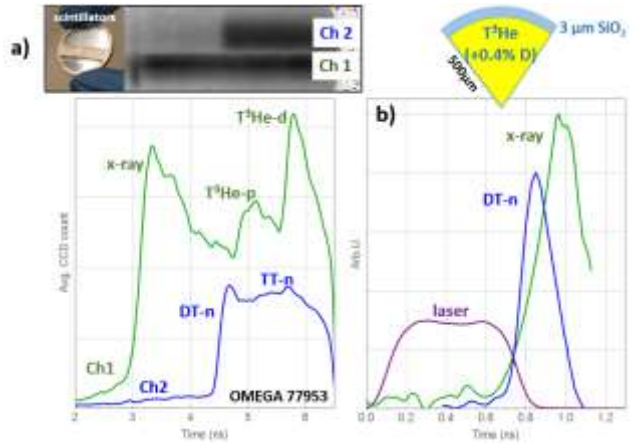

Figure 8: a) A proof-of-principle PXTD measurement of charged particles, neutrons, and x-ray signals from a THe^3-gas-filled implosion (with 0.4% D contamination). a) The top streak image illustrates the streak signals of x-rays, T^3He-p, and T^3He-d on channel 1, and the streak signals of DT-n and TT-n on channel 2. The bottom plot illustrates the lineouts (the streak image projected onto the time axis). b) The DT-n reaction and x-ray (>12 keV) emission history are relatively timed to each other to within ± 10 ps, and absolutely timed to the laser drive. The 14.1-MeV DT-n and 9.5-MeV T^3He-d are monoenergetic particles, whereas the T^3He-p and the TT-n have broad, continuous energy spectrum. Ch1 is filtered with 40-μm Ta + 40-μm Al, and Ch2 is filtered with 540-μm Ta + 40-μm Al.

The ultimate goal with the PXTD is to provide simultaneous high-precision, time-resolved measurements of several nuclear reactions and the x-ray core continuum. This involves measurements of nuclear reaction and x-ray emission histories using the same streak camera. As already discussed, measurements of both the x-ray emission and nuclear reactions are undertaken using three different channels, but it also helps that they arrive at the PXTD scintillator at different times and thus temporally separated from each other. X-rays', D^3He-p's, and DD-n's time-of-flight to the scintillator, positioned 9 cm from the implosion, is 0.3 ns, 1.7 ns, and 4.2 ns, respectively. Careful selection of filters in front of the different scintillator channels allows simultaneous and optimized measurements of x-rays, charged particles and neutrons. Typically, 1D radiation-hydrodynamic simulations (HYADES[12]) are used to anticipate

the particle and x-ray signal levels and design the PXTD filter setup.

An example of simultaneous measurements of x-rays, charged particles, and neutrons is shown in Figure 8a. This data was obtained from a T^3He gas-filled implosion with 0.4% D. For channel 1, the filter was used to simultaneously measure x-rays above 12 keV, T^3He-d, and T^3He-p. For channel 2, a filter was used to measure both DT-neutrons and TT-neutrons. Figure 8b shows the DT-n reaction and x-ray emission histories, determined from the data shown in Figure 8a, with relative timing uncertainty within ± 10 ps, and absolutely timed to the laser drive. This enables studies of x-ray bang-time, nuclear bang-time, and their time difference in different ICF plasma conditions.

IV. ANALYSIS METHODS AND UNCERTAINTIES

A. ANALYSIS METHODS

As discussed to some extent in previous sections, the analysis of the signal lineouts involves a forward-fit or a deconvolution approach. In the forward fit method, the scintillator response, Doppler broadening, instrumental broadening, and the assumed source function are convolved and fitted to the data iteratively until a best fit is found. Generally, a linear combination of skewed Gaussians is used as the source reaction history for the forward fit analysis. In thin-glass shock-driven exploding pushers which have little compression yield, a single skewed Gaussian adequately describes the data. For more compressively driven implosions, two skewed Gaussians may be used, one for thermonuclear burn during shock flash, and another for thermonuclear burn during compression.

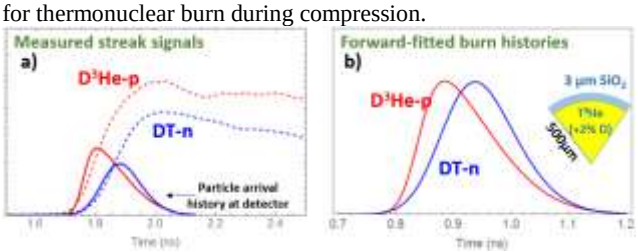

Figure 9: a) Measured D^3He- and DT streak lineouts (dashed) and deconvolved signals (solid) representing the particle arrival histories at the PXTD scintillator. In this case, the DT-n and D^3He-p burn histories are simultaneously determined with a relative precision of ~10 ps for this thin-glass shock-driven implosion with T_2 + ^3He fill, with a trace amount of D_2. The forward-fitted D^3He-p and DT-n burn histories shown in b), normalized to illustrated differences in shape.

When applying the deconvolution approach[11] to the data, the exponential decay of the scintillator light emission is removed from the streaked signal lineout. This deconvolved signal represents the arrival history of the charged particles neutrons, or x-rays at the scintillator, and is used to determine the Doppler-broadened source function for charged particles or neutrons, or the source function for x-rays. These two analysis methods provide the same answers in terms of inferred bang time, burn duration and burn onset. In practice, both analysis methods are used to quantify sensitivities to different analysis techniques.

An understanding of the time-integrated energy spectrum for the relevant nuclear fusion products (D^3He-p, DT-n, DD-n) is essential for the determination of the absolute and relative timing for the different nuclear-reaction histories. In the case of DT-n and DD-n, the Doppler-broadened spectrum is used to calculate the time-of-flight to the detector [Ballabio *et al*[13]]. In the case of D^3He-p, at least three charged-particle spectrometers (Wedge-Range-Filter[14], Charged-Particles-Spectrometer[15]) are fielded for on-shot measurements of the D^3He-p proton spectrum.

B. UNCERTAINTIES

As the timing of the simulated burn onsets, bang times and complete reaction histories vary with ~30-50 ps depending on what simulation method is used (single-ion-fluid and multi-ion-fluid simulation)[16], the relative timing precision needed to differentiate them is ~ 20-25 ps. This can be achieved with the PXTD as summarized by Table 1.

Depending on the velocity of the charged-particles, neutrons, and x-rays, they arrive at different times at the scintillator, and the uncertainty in their velocity and time-of-flight times translates directly into an uncertainty in relative timing between the different signals. An energy uncertainty of 100 keV for the 14.7-MeV D^3He-p translates into ~ 10 ps timing uncertainty (systematic and random). For DT-n and DD-n, an energy uncertainty of ~ 10 keV translates to timing uncertainties of 1 ps and 8 ps, respectively. The time-of-flight uncertainty is zero for x-rays, as they travel at the speed of light.

Table 1: Summary of systematic and random timing uncertainties for the PXTD, positioned at 3 cm and 9 cm from the implosion for measurements of D^3He-p bang-time relative to DT-n, DD-n, or x-ray bang times. D^3He-p is assumed to have an energy of 14.7 MeV, with an uncertainty of 100 keV. DT-n and DD-n are assumed to have an energy uncertainty of 10 keV.

Uncertainty sources	**Δ(bang-time) uncertainty (ps) between**			
	D^3He-p and x-ray	**D^3He-p and DT-n**	**D^3He-p and DD-n**	**D^3He-p and DD-n**
Random	at 9 cm	at 9 cm	at 3 cm	at 9 cm
D^3He-p TOF	5	5	5	5
Neutron TOF	~	< 1	3	8
Sweep nonlinearity	5	< 5	5	5
Photon statistics	< 5	< 5	5-10	10-15
Fitting	0-5	0-5	0-10	5-10
Total (random)	5-10	5-10	10-15	15-25
Systematic				
D^3He-p TOF	5	5	5	5
distance	3	< 1	3	8
Total (systematic)	5	5	6	10

For DD-n, the major contribution to timing uncertainty is limited photon statistics. At 9 cm from the implosion, a minimum DD-n yield of 3e10 is required to accurately measure the reaction history. If the signal is significantly Doppler-broadened (such as for DD-n), this further exacerbates the problem. DT-n and charged-particle measurements are usually not limited by photon statistics because of much higher signal levels at the streak camera. Other sources of uncertainties not discussed in detail are sweep nonlinearity (partially corrected using the OMEGA fiducial pulses), and distance uncertainty (from the implosion).

As show by Table 1, a reduction of the relative timing uncertainty between nuclear reaction histories is achieved by using higher-velocity particles. Using DT-n also has the advantage that higher signal levels are obtained, which improves statistics. Another approach to reduce the timing uncertainty is to

move the scintillator(s) closer to the implosion, which will be discussed in the next section.

V. In-close PXTD

Moving the PXTD scintillator closer to the implosion is advantageous because of a smaller absolute uncertainty associated with a reduced time-of-flight, and improved photon statistics per time bin from reduced temporal broadening. A new PXTD nosecone design has been completed. This design will position the scintillators at 3 cm from the implosion, significantly improving the quality of the DD-n reaction history measurement. This new configuration has the same solid angle as the 9-cm design, which means that it can only accommodate two streak channels (see Figure 10). Three additional lenses have been added in the new nosecone to relay scintillator light from the new input plane at 3 cm.

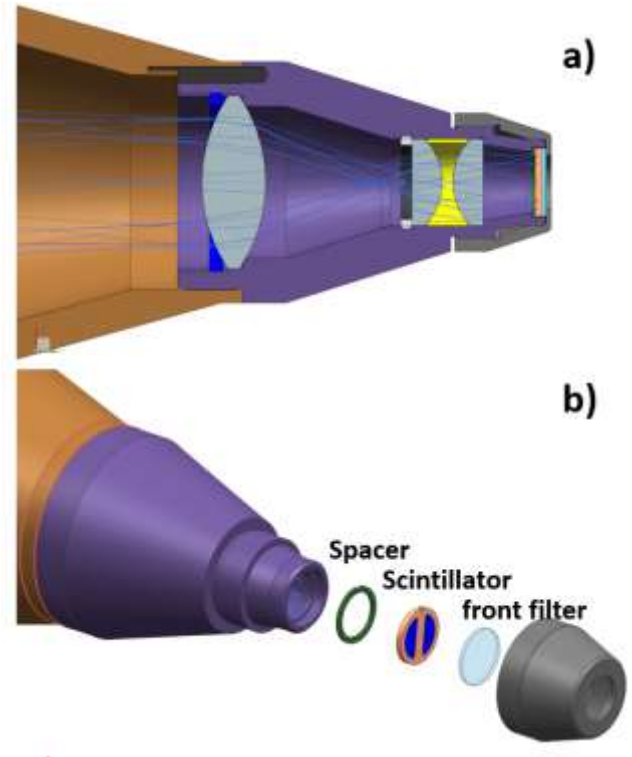

Figure 10: a) Sliced view of the new 3-cm PXTD nosecone design. Three new lens are added in the new (purple) nosecone to relay light from the new scintillator plane at 3 cm. b) Exploded view of the new 3-cm PXTD nosecone design. Because of space constraints only two streak channels can be accommodated.

For a shock-driven implosion with a 10 keV ion temperature, Doppler broadening is the dominant temporal broadening source. At 9 cm, a DD-n burn history with 150 ps FWHM will be broadened to 270 ps FWHM. At 3 cm, the final FWHM including Doppler broadening is only 175 ps. The D^3He-p and DT-n burn histories are not significantly affected by the Doppler broadening because of their much higher velocities.

VII. CONCLUSION AND FUTURE WORK

A Particle X-Ray Temporal Diagnostic (PXTD) has been implemented and extensively used at OMEGA for simultaneous measurements of nuclear-reaction and x-ray emission histories. Three streak channels, with individual x-ray filters and light attenuation filters, provide flexibility in measuring different charged-particles, neutrons, and x-ray emission histories with high relative timing precision ~ ± 10-20 ps. From the measured nuclear reaction histories, an assessment of kinetic and multi-ion-fluid effects in ICF plasmas can be made. Ongoing work focuses on optimization of the PXTD for simultaneous measurements of two nuclear reaction histories and three x-ray emission histories, from which $T_i(t)$ and $T_i(t)$ and thus ion-electron equilibration rates can be inferred. Quantitative changes in nuclear reaction histories as implosion transitions from hydrodynamic-like to more kinetic regime will also be compared with multi-ion-fluid and kinetic-ion simulations (such as LSP[17]) in the near future.

VIII. ACKNOWLEDGMENTS

This work was supported in part by the (U.S.) Department of Energy (DOE) (DE-NA0002949), Laboratory for Laser Energetics (416107-G) and the National Laser Users Facility (DE-NA0002726). H. Sio is supported by the DOE NNSA Stewardship Science Graduate Fellowship (DE-FC52-08NA28752).

IX. REFERENCES AND FOOTNOTES

1. Rosenberg, M. J. *et al.* Exploration of the transition from the hydrodynamiclike to the strongly kinetic regime in shock-driven implosions. *Phys.Rev.Lett.* **112,** 185001 (2014).

2. Rinderknecht, H. G. *et al.* Ion Thermal Decoupling and Species Separation in Shock-Driven Implosions. *Phys. Rev. Lett.* **114,** 025001 (2015).

3. Rygg, J. R. *et al.* Tests of the hydrodynamic equivalence of direct-drive implosions with different D2 and 3He mixtures. *Phys. Plasmas* **13,** 052702 (2006).

4. Herrmann, H. W. *et al.* Anomalous yield reduction in direct-drive deuterium / tritium implosions due to 3 He addition a …. *Phys. Plasmas* **052706,** 1–9 (2009).

5. Rinderknecht, H. G. G. *et al.* First Observations of Nonhydrodynamic Mix at the Fuel-Shell Interface in Shock-Driven Inertial Confinement Implosions. *Phys. Rev. Lett.* **112,** 135001 (2014).

6. Casey, D. T. *et al.* Evidence for Stratification of Deuterium-Tritium Fuel in Inertial Confinement Fusion Implosions. *Phys. Rev. Lett.* **108,** 075002 (2012).

7. Boehly, T. R. *et al.* Initial performance results of the OMEGA laser system. *Opt. Commun.* **133,** 495–506 (1997).

8. Frenje, J. A., Li, C. K., Séguin, F. H., Deciantis, J. & Kurebayashi, S. Measuring shock-bang timing and R evolution of D3He implosions at OMEGA Measuring shock-bang timing and □ R evolution of D 3 He implosions at OMEGA a …. **2798,** (2011).

9. Lerche, R. A. *et al.* 25 ps neutron detector for measuring ICFtarget burn history detector for measuring. **933,** 1–4 (2012).

10. Campbell, E. M., Hunt, J. T., Bliss, E. S., Speck, D. R. & Drake, R. P. Nova experimental facility. *Rev. Sci. Instrum.* **57,** (1986).

11. Stoeckl, C. *et al.* Ten-inch manipulator-based neutron temporal diagnostic for cryogenic experiments on OMEGA Ten-inch manipulator-based neutron temporal diagnostic for cryogenic experiments on OMEGA. **1713,** (2012).

12. Larsen, J. T. & Lane, S. M. HYADES—A plasma hydrodynamics code for dense plasma studies. *J. Quant. Spectrosc. Radiat. Transf.* **51,** 179–186 (1994).

13. L. Ballabio, J. Kallne, G. G. Relativistic calculation of fusion product spectra for thermonuclear plasmas. *Nucl. Fusion* **38,** (1998).

14. Seguin, F. H. *et al*. Advances in compact proton spectrometers for inertial-confinement fusion and plasma nuclear science a). **908,** 3–5 (2012).

15. Seguin, F. H. *et al*. Spectrometry of charged particles from inertial-confinement-fusion plasmas. **74,** 975–995 (2003).

16. Bellei, C. *et al*. Species separation and kinetic effects in collisional plasma shocksa). *Phys. Plasmas* **21,** 56310 (2014).

17. Welch, D. R., Rose, D. V., Clark, R. E., Genoni, T. C. & Hughes, T. P. Implementation of an non-iterative implicit electromagnetic field solver for dense plasma simulation. *Comput. Phys. Commun.* **164,** 183–188 (2004).